

Chapter 30

Turbulence?

I am an old man now, and when I die and go to Heaven there are two matters on which I hope enlightenment. One is quantum electro-dynamics and the other is turbulence of fluids. About the former, I am rather optimistic.

—Sir Horace Lamb

THERE IS ONLY ONE honorable cause that would justify sweating through so much formalism - this is but the sharpening of a pencil in order that we may attack the Navier-Stokes equation,

$$\frac{\partial \mathbf{u}}{\partial t} + \mathbf{u} \cdot \nabla \mathbf{u} = -\frac{\nabla p}{\rho} + \nu \nabla^2 \mathbf{u} + \mathbf{f}, \tag{30.1}$$

and solve the problem of turbulence.

Being realistic, we are not so foolhardy to immediately plunge into *the* problem – there are too many dimensions and indices. Instead, we start small, in one spatial dimension, $\mathbf{u} \rightarrow u$, $\mathbf{u} \cdot \nabla \mathbf{u} \rightarrow u \partial_x u$, assume constant density ρ , forget about the pressure p , and so on. This line of reasoning, as well as many other equally sensible threads of thought, such as the amplitude equations obtained via weakly nonlinear stability analysis of steady flows, leads to a small set of frequently studied nonlinear PDE models, like the one that we turn to now. You only need chapters 2 to 5 and chapters 14 to 15 to get started.

30.1 Configuration space: a fluttering flame front

Romeo: ‘Misshapen chaos of well seeming forms!’
—W. Shakespeare, *Romeo and Julliet*, Act I, Scene I

The Kuramoto-Sivashinsky [KS] system describes the flame front flutter of gas burning on your kitchen stove, figure 30.1 (a), and many other problems of



greater import, is one of the simplest nonlinear systems that exhibit ‘turbulence’ (in this context often referred to more modestly as ‘spatiotemporally chaotic behavior’). The time evolution of the ‘flame front velocity’ $u = u(x, t)$ on a periodic domain $u(x, t) = u(x + L, t)$ is given by

$$u_t + \frac{1}{2}(u^2)_x + u_{xx} + \nu u_{xxxx} = 0, \quad x \in [0, L]. \tag{30.2}$$

In this equation $t \geq 0$ is the time and x is the spatial coordinate. The subscripts x and t denote partial derivatives with respect to x and t : $u_t = \partial u / \partial t$, u_{xxxx} stands for the 4th spatial derivative of $u = u(x, t)$ at position x and time t . In what follows we use interchangeably the ‘dimensionless system size’ \tilde{L} , or the periodic domain size $L = 2\pi\tilde{L}$, as the system parameter. We take note, as in the Navier-Stokes equation (30.1), of the ‘inertial’ term $u \partial_x u$, the ‘anti-diffusive’ term $\partial_x^2 u$ (with a “wrong” sign), ‘(hyper-)viscosity’ ν , etc..

In what follows we will analyse -step by step- PDEs using methods developed above for finite dimensional dynamical systems. First we discuss PDEs as fields defined over configuration space. Once we go over to the state space description the techniques developed for analysis of ODEs will go over to PDEs, as is.

30.1.1 The Ring of Fire - symmetries

The Kuramoto-Sivashinsky equation (30.2) is space translationally invariant, time translationally invariant, and invariant under reflection $x \rightarrow -x$, $u \rightarrow -u$. Comparing u_t and $(u^2)_x$ terms we note that u has dimensions of $[x]/[t]$, hence u is the ‘velocity’, rather than the ‘height’ of the flame front. Indeed, the Kuramoto-Sivashinsky equation is Galilean invariant: if $u(x, t)$ is a solution, then $v + u(x - vt, t)$, with v an arbitrary constant velocity, is also a solution. Without loss of generality, in our calculations we shall work in the zero mean velocity frame

$$\int dx u = 0. \tag{30.3}$$

In terms of the system size L , the only length scale available, the dimensions of terms in (30.2) are $[x] = L$, $[t] = L^2$, $[u] = L^{-1}$, $[\nu] = L^2$. Scaling out the “viscosity” ν by $x \rightarrow xv^{1/2}$, $t \rightarrow tv$, $u \rightarrow uv^{-1/2}$, brings the Kuramoto-Sivashinsky equation (30.2) to a non-dimensional form

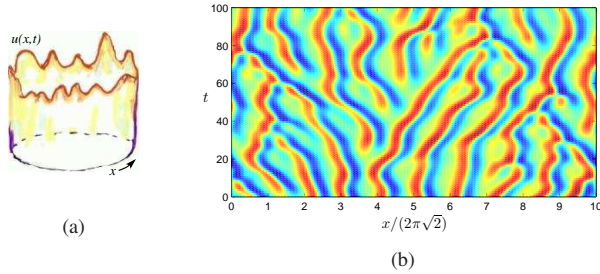
$$u_t + u u_x + u_{xx} + u_{xxxx} = 0, \quad x \in [0, Lv^{-1/2}] = [0, 2\pi\tilde{L}]. \tag{30.4}$$

In this way we trade in the “viscosity” ν and the system size L for a single dimensionless system size parameter

$$\tilde{L} = L/(2\pi\sqrt{\nu}) \tag{30.5}$$

which plays the role of a “Reynolds number” for the Kuramoto-Sivashinsky system. Sometimes L is used as the system parameter, with ν fixed to 1, and at other times ν is varied with L fixed to either 1 or 2π . Physically, varying L is the right thing to do if one is interested in taking L large, and studying ‘spatio-temporal

Figure 30.1: (a) Kuramoto-Sivashinsky dynamics visualized as the Bunsen burner flame flutter, with $u = u(x, t)$ the “velocity of the flame front” at position x and time t . (b) A typical “turbulent” solution of the Kuramoto-Sivashinsky equation, system size $L = 20\pi\sqrt{2} \approx 88.86$. The color (gray scale) indicates the value of u at a given position and instant in time. The x coordinate is scaled with the most unstable wavelength $2\pi\sqrt{2}$, which is approximately also the mean wavelength of the turbulent flow. The dynamics is typical of a large system, in this case approximately 10 mean wavelengths wide. (from ref. [A1.84])



chaos.’ In what follows we shall state results of all calculations in units of dimensionless system size \tilde{L} . The time units also have to be rescaled; for example, if T_p^* is a period of a periodic solution of (30.2) with a given ν and $L = 2\pi$, then the corresponding solution of the non-dimensionalized (30.4) has period

$$T_p = T_p^* / \nu. \tag{30.6}$$

The term $(u^2)_x$ makes this a *nonlinear system*. This is one of the simplest conceivable nonlinear PDE, playing the role in the theory of spatially extended systems a bit like the role that the x^2 nonlinearity plays in the dynamics of iterated mappings. The time evolution of a typical solution of the Kuramoto-Sivashinsky system is illustrated by figure 30.1 (b).

section 3.3
remark 30.1

G , the group of actions $g \in G$ on a state space (reflections, translations, etc.) is a symmetry of the KS flow (30.2) if $g u_t = F(g u)$. The KS equation is time translationally invariant, and space translationally invariant on a periodic domain under the 1-parameter group of $O(2) : \{\tau_{\ell/L}, \sigma\}$. If $u(x, t)$ is a solution, then $\tau_{\ell/L} u(x, t) = u(x + \ell, t)$ is an equivalent solution for any shift $-L/2 < \ell \leq L/2$, as is the reflection (‘parity’ or ‘inversion’)

$$\sigma u(x) = -u(-x). \tag{30.7}$$

Due to the hyperviscous damping u_{xxxx} , long time solutions of Kuramoto-Sivashinsky equation are smooth, a_k drop off fast with k , and truncations of (30.13) to N terms, $16 \leq N \leq 128$, yield highly accurate solutions for system sizes considered here. Robustness of the Fourier representation of KS as a function of the number of modes kept in truncations, a subtle issue. Adding an extra mode to a truncation introduces a small perturbation. However, this can (and often will) throw the dynamics into a different asymptotic state. A chaotic attractor for $N = 15$ can collapse into an attractive period-3 cycle for $N = 16$, and so on.

If we compute, for example, the Lyapunov exponent λ_N for a strange attractor of the system (30.13), there is no reason to expect λ_N to smoothly converge to a limit value λ , as $N \rightarrow \infty$, because of the lack of structural stability both as a function of truncation N , and the system size \tilde{L} . However, later in this chapter we explore both equilibria and short periodic orbits, which are robust under mode truncations and small system parameter \tilde{L} changes. Spatial representations of PDEs (such as figure 30.1 (b) and the 3D snapshots of velocity and vorticity fields in Navier-Stokes) offer little insight into detailed dynamics of low- Re flows. Much more illuminating are the state space representations.

 example 30.1
p. 584

Reflection generates the dihedral subgroup $D_1 = \{1, \sigma\}$ of $O(2)$. Let \mathbb{U} be the space of real-valued velocity fields periodic and square integrable on the interval $\Omega = [-L/2, L/2]$,

$$\mathbb{U} = \{u \in L^2(\Omega) \mid u(x) = u(x + L)\}. \tag{30.8}$$

A continuous symmetry maps each state $u \in \mathbb{U}$ to a manifold of functions with identical dynamic behavior. Relation $\sigma^2 = 1$ induces linear decomposition $u(x) = u^+(x) + u^-(x)$, $u^\pm(x) = P^\pm u(x) \in \mathbb{U}^\pm$, into irreducible subspaces $\mathbb{U} = \mathbb{U}^+ \oplus \mathbb{U}^-$, where

$$P^+ = (1 + \sigma)/2, \quad P^- = (1 - \sigma)/2, \tag{30.9}$$

are the antisymmetric/symmetric projection operators. Applying P^+ , P^- on the KS equation (30.2) we have [30.17]

$$\begin{aligned} u_t^+ &= -(u^+ u_x^+ + u^- u_x^-) - u_{xx}^+ - u_{xxxx}^+ \\ u_t^- &= -(u^+ u_x^- + u^- u_x^+) - u_{xx}^- - u_{xxxx}^-. \end{aligned} \tag{30.10}$$

If $u^- = 0$, KS flow is confined to the antisymmetric \mathbb{U}^+ subspace,

$$u_t^+ = -u^+ u_x^+ - u_{xx}^+ - u_{xxxx}^+, \tag{30.11}$$

but otherwise the nonlinear terms in (30.10) mix the two subspaces.

 example 30.2
p. 584

30.2 Constructing a state space

Spatial periodicity $u(x, t) = u(x + L, t)$ makes it convenient to work in the Fourier space,

$$u(x, t) = \sum_{k=-\infty}^{+\infty} a_k(t) e^{ikx/\tilde{L}}, \tag{30.12}$$

with the 1-dimensional PDE (30.2) replaced by an infinite set of ODEs for the complex Fourier coefficients $a_k(t)$:

$$\dot{a}_k = v_k(a) = (q_k^2 - q_k^4) a_k - i \frac{q_k}{2} \sum_{m=-\infty}^{+\infty} a_m a_{k-m}, \quad q_k = k/\tilde{L}. \quad (30.13)$$

As $\dot{a}_0 = 0$, a_0 is a conserved quantity, in our calculations fixed to $a_0 = 0$ by the vanishing mean $\langle u \rangle$ condition (30.3) for the front velocity. The velocity field $u(x, t)$ is real, so $a_k = a_{-k}^*$, and we can replace the sum by an $m > 0$ sum. This is the infinite set of ordinary differential equations promised in this chapter's introduction.

As $\dot{a}_0 = 0$ in (30.13), a_0 is a conserved quantity fixed to $a_0 = 0$ by the condition (30.3).

The translation operator action on the Fourier coefficients (2.16), represented here by a complex valued vector $a = \{a_k \in \mathbb{C} | k = 1, 2, \dots\}$, is given by

$$\tau_{\ell/L} a = \mathbf{g}(\ell) a, \quad (30.14)$$

where $\mathbf{g}(\ell) = \text{diag}(e^{iq_k \ell})$ is a complex valued diagonal matrix, which amounts to the k -th mode complex plane rotation by an angle $k \ell / \tilde{L}$. The reflection acts on the Fourier coefficients by complex conjugation,

$$\sigma a = -a^*. \quad (30.15)$$

30.2.1 Equilibria and relative equilibria

Equilibria (or the steady solutions) are the fixed profile time-invariant solutions,

$$u(x, t) = u_q(x). \quad (30.16)$$

Due to the translational symmetry, the KS system also allows for relative equilibria (traveling waves, rotating waves), characterized by a fixed profile $u_q(x)$ moving with constant speed c , i.e.

$$u(x, t) = u_q(x - ct). \quad (30.17)$$

Here suffix q labels a particular invariant solution. Because of the reflection symmetry (30.7), the relative equilibria come in counter-traveling pairs $u_q(x - ct)$, $-u_q(-x + ct)$.

The relative equilibrium condition for the Kuramoto-Sivashinsky PDE (30.2) is the ODE

$$\frac{1}{2}(u^2)_x + u_{xx} + u_{xxxx} = c u_x \quad (30.18)$$

which can be analyzed as a dynamical system in its own right. Integrating once we get

$$\frac{1}{2}u^2 - cu + u_x + u_{xxx} = E. \quad (30.19)$$

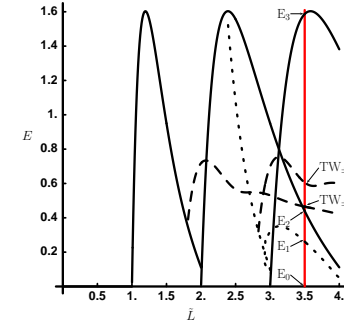


Figure 30.2: The energy (30.31) of the equilibria and relative equilibria that exist up to $L = 22$, $\tilde{L} = 3.5014 \dots$, plotted as a function of the system size $\tilde{L} = L/2\pi$ (additional equilibria, not present at $L = 22$ are given in ref. [30.9]). Solid curves denote n -cell solutions EQ_2 and EQ_3 , dotted curves the GLMRT equilibrium EQ_1 , and dashed curves the relative equilibria $TW_{\pm 1}$ and $TW_{\pm 2}$. The parameter α of refs. [30.17, 30.9] is related to the system size by $\tilde{L} = \sqrt{\alpha/4}$.

This equation can be interpreted as a 3-dimensional dynamical system with spatial coordinate x playing the role of 'time,' and the integration constant E can be interpreted as 'energy,' see sect. 30.3.

For $E > 0$ there is rich E -dependent dynamics, with fractal sets of bounded solutions investigated in depth by Michelson [30.18]. For $\tilde{L} < 1$ the only equilibrium of the system is the globally attracting constant solution $u(x, t) = 0$, denoted EQ_0 from now on. With increasing system size L the system undergoes a series of bifurcations. The resulting equilibria and relative equilibria are described in the classical papers of Kevrekidis, Nicolaenko and Scovel [30.17], and Greene and Kim [30.9], among others. The relevant bifurcations up to the system size investigated here are summarized in figure 30.2: at $\tilde{L} = 22/2\pi = 3.5014 \dots$, the equilibria are the constant solution EQ_0 , the equilibrium EQ_1 called GLMRT by Greene and Kim [?, 30.9], the 2- and 3-cell states EQ_2 and EQ_3 , and the pairs of relative equilibria $TW_{\pm 1}$, $TW_{\pm 2}$. All equilibria are in the antisymmetric subspace \mathbb{U}^+ , while EQ_2 is also invariant under D_2 and EQ_3 under D_3 .

In the Fourier representation the relative equilibria time dependence is

$$a_k(t) e^{-itcq_k} = a_k(0). \quad (30.20)$$

Differentiating with respect to time, we obtain the Fourier space version of the relative equilibrium condition (30.18),

$$v_k(a) - iq_k c a_k = 0, \quad (30.21)$$

which we solve for (time independent) a_k and c .

Periods of spatially periodic equilibria are multiples of L . Every time the system size crosses $\tilde{L} = n$, n -cell states are generated through pitchfork bifurcations

off $u = 0$ equilibrium. Due to the translational invariance of Kuramoto-Sivashinsky equation, they form invariant circles in the full state space. In the \mathbb{U}^+ subspace considered here, they correspond to $2n$ points, each shifted by $L/2n$. For a sufficiently small L the number of equilibria is small and concentrated on the low wave-number end of the Fourier spectrum.

From (30.13) we see that the origin $u(x, t) = 0$ has Fourier modes as the linear stability eigenvectors. The $|k| < \tilde{L}$ long wavelength perturbations of the flat-front equilibrium are linearly unstable, while all $|k| > \tilde{L}$ short wavelength perturbations are strongly contractive. The high k eigenvalues, corresponding to rapid variations of the flame front, decay so fast that the corresponding eigendirections are physically irrelevant. The most unstable mode, nearest to $|k| = \tilde{L}/\sqrt{2}$, sets the scale of the mean wavelength $\sqrt{2}$ of the KS ‘turbulent’ dynamics, see figure 30.1.

30.2.2 Relative periodic orbits, symmetries and periodic orbits

The KS equation (30.2) is time translationally invariant, and space translationally invariant under the $1-d$ Lie group of $O(2)$ rotations: if $u(x, t)$ is a solution, then $u(x + \ell, t)$ and $-u(-x, t)$ are equivalent solutions for any $-L/2 < \ell \leq L/2$. As a result of invariance under $\tau_{\ell/L}$, KS equation can have relative periodic orbit solutions with a profile $u_p(x)$, period T_p , and a nonzero shift ℓ_p

$$\tau_{\ell_p/L} u(x, T_p) = u(x + \ell_p, T_p) = u(x, 0) = u_p(x). \quad (30.22)$$

Relative periodic orbits (30.22) are periodic in $v_p = \ell_p/T_p$ co-rotating frame (see figure 12.7), but in the stationary frame their trajectories are quasiperiodic. Due to the reflection symmetry (30.7) of KS equation, every relative periodic orbit $u_p(x)$ with shift ℓ_p has a symmetric partner $-u_p(-x)$ with shift $-\ell_p$.

Due to invariance under reflections, KS equation can also have relative periodic orbits *with reflection*, which are characterized by a profile $u_p(x)$ and period T_p

$$\sigma u(x + \ell, T_p) = -u(-x - \ell, T_p) = u(x + \ell, 0) = u_p(x), \quad (30.23)$$

giving the family of equivalent solutions parameterized by ℓ (as the choice of the reflection point is arbitrary, the shift can take any value in $-L/2 < \ell \leq L/2$).

Armbruster *et al.* [?, 12.16] and Brown and Kevrekidis [12.21] (see also ref. [13.60]) link the birth of relative periodic orbits to an infinite period global bifurcation involving a heteroclinic loop connecting equilibria or a bifurcation of relative equilibria, and also report creation of relative periodic orbit branches through bifurcation of periodic orbits.

As ℓ is continuous in the interval $[-L/2, L/2]$, the likelihood of a relative periodic orbit with $\ell_p = 0$ shift is zero, unless an exact periodicity is enforced by a discrete symmetry, such as the dihedral symmetries discussed above. If the shift ℓ_p of a relative periodic orbit with period T_p is such that ℓ_p/L is a rational

number, then the orbit is periodic with period nT_p . The likelihood to find such periodic orbits is also zero.

However, due to the KS equation invariance under the dihedral D_n and cyclic C_n subgroups, the following types of periodic orbits are possible:

(a) The periodic orbit lies within a subspace pointwise invariant under the action of D_n or C_n . For instance, for D_1 this is the \mathbb{U}^+ antisymmetric subspace, $-u_p(-x) = u_p(x)$, and $u(x, T_p) = u(x, 0) = u_p(x)$. The periodic orbits found in refs. [A1.79, 30.23] are all in \mathbb{U}^+ , as the dynamics is restricted to antisymmetric subspace. For $L = 22$ the dynamics in \mathbb{U}^+ is dominated by attracting (within the subspace) heteroclinic connections and thus we have no periodic orbits of this type, or in any other of the D_n -invariant subspaces, see sect. ??.

(b) The periodic orbit satisfies

$$u(x, t + T_p) = \gamma u(x, t), \quad (30.24)$$

for some group element $\gamma \in O(2)$ such that $\gamma^m = e$ for some integer m so that the orbit repeats after time mT_p (see ref. [12.4] for a general discussion of conditions on the symmetry of periodic orbits). If an orbit is of reflection type (30.23), $\sigma \tau_{\ell/L} u(x, T_p) = -u(-x - \ell, T_p) = u(x, 0)$, then it is pre-periodic to a periodic orbit with period $2T_p$. Indeed, since $(\sigma \tau_{\ell/L})^2 = \sigma^2 = 1$, and the KS solutions are time translation invariant, it follows from (30.23) that

$$u(x, 2T_p) = \sigma \tau_{\ell/L} u(x, T_p) = (\sigma \tau_{\ell/L})^2 u(x, 0) = u(x, 0).$$

Thus any shift acquired during time 0 to T_p is compensated by the opposite shift during evolution from T_p to $2T_p$. All periodic orbits we have found for $L = 22$ are of type (30.24) with $\gamma = R$. Pre-periodic orbits with $\gamma \in C_n$ have been found by Brown and Kevrekidis [12.21] for KS system sizes larger than ours, but we have not found any for $L = 22$. Pre-periodic orbits are a hallmark of any dynamical system with a discrete symmetry, where they have a natural interpretation as periodic orbits in the fundamental domain.

30.3 Energy budget

Mathematical physics is three things: Gaussian integrals, integration by parts and ... (nobody remembers exactly what the third thing was, including Joel).

—Joel Lebowitz, in a seminar

In physical settings where the observation times are much longer than the dynamical ‘turnover’ and Lyapunov times (statistical mechanics, quantum physics, turbulence) periodic orbit theory provides highly accurate predictions of measurable long-time averages such as the dissipation and the turbulent drag. Physical predictions have to be independent of a particular choice of ODE representation of the PDE under consideration and invariant under all symmetries of the dynamics. In this section we discuss a set of such physical observables for the $1-d$ KS

invariant under reflections and translations. Here we shall show that they offer a visualization of solutions of dynamics in which the symmetries are explicitly quotiented out.

The *space average* of a function $a = a(x, t) = a(u(x, t))$ periodic on the interval L is given by

$$\langle a \rangle = \frac{1}{L} \oint dx a(x, t), \quad (30.25)$$

We note that total derivatives vanish by the spatial periodicity on the L domain, and that by integration by parts

$$\langle f_x \rangle = 0, \quad \langle f_x g \rangle = -\langle f g_x \rangle \quad (30.26)$$

for any L -periodic functions f, g . In general $\langle a \rangle$ is time dependent. Its *mean value* is given by the *time average*

$$\bar{a} = \lim_{t \rightarrow \infty} \frac{1}{t} \int_0^t d\tau \langle a \rangle = \lim_{t \rightarrow \infty} \frac{1}{t} \int_0^t \frac{1}{L} \oint dx a(x, \tau). \quad (30.27)$$

The mean value of $a_q = a(u_q)$ evaluated on equilibrium or relative equilibrium $u(x, t) = u_q(x - ct)$, is

$$\bar{a}_q = \langle a \rangle_q = a_q. \quad (30.28)$$

Evaluation of the infinite time average (30.27) on a function of a periodic orbit or relative periodic orbit $u_p(x, t) = u_p(x + \ell_p, t + T_p)$ requires only a single T_p traversal,

$$\bar{a}_p = \frac{1}{T_p} \int_0^{T_p} d\tau \langle a \rangle. \quad (30.29)$$

Equation (30.2) can be written as

$$u_t = -V_x, \quad V(x, t) = \frac{1}{2}u^2 + u_x + u_{xxx}, \quad (30.30)$$

and E can be interpreted as the mean energy density (30.31). So, even though KS is a phenomenological small-amplitude equation, the time-dependent L^2 norm of u (simplified using integration by parts, as in (30.26)),

$$E = \frac{1}{L} \oint dx V(x, t) = \frac{1}{L} \oint dx \frac{u^2}{2}, \quad (30.31)$$

has a physical interpretation as the average ‘energy’ density of the flame front. This analogy to the mean kinetic energy density for the Navier-Stokes motivates what follows.

The energy (30.31) is intrinsic to the flow, independent of the particular ODE basis set chosen to represent the PDE. As the Fourier amplitudes are eigenvectors of the translation operator, in the Fourier space the energy is a diagonalized quadratic norm,

$$E = \sum_{k=1}^{\infty} E_k, \quad E_k = \frac{1}{2}|a_k|^2, \quad (30.32)$$

Figure 30.3: Power input $\langle u_x^2 \rangle$ vs. dissipation $\langle u_{xx}^2 \rangle$ for $L = 22$ equilibria and relative equilibria, for several periodic orbits and relative periodic orbits, and for a typical ‘turbulent’ state. Note that $\overline{\langle u_{p,x} \rangle^2}$ of the $(T_p, \ell_p) = (32.8, 10.96)$ relative periodic orbit which appears well embedded within the turbulent state, is close to the turbulent expectation $\overline{\langle u_x \rangle^2}$.

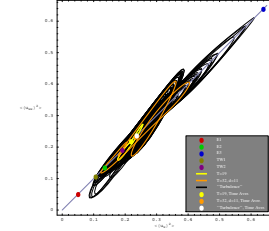
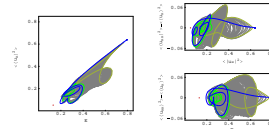


Figure 30.4: EQ_1 (red), EQ_2 (green), EQ_3 (blue), connections from EQ_1 to $A(L/4)EQ_1$ (green), from $A(L/4)EQ_1$ to EQ_1 (yellow-green) and from EQ_3 to $A(L/4)EQ_1$ (blue), along with a generic long-time ‘turbulent’ evolution (grey) for $L = 22$. Three different projections of the $(E, \langle u_x^2 \rangle, \langle u_{xx}^2 \rangle - \langle u_x^2 \rangle)$ representation are shown.



and explicitly invariant term by term under translations and reflections.

Take time derivative of the energy density (30.31), substitute (30.2) and integrate by parts, as in (30.26):

$$\begin{aligned} \dot{E} &= \langle u_t u \rangle = -\langle (u^2/2 + u_x + u_{xxx})_x u \rangle \\ &= \langle u_x u^2/2 + u_x^2 + u_x u_{xxx} \rangle. \end{aligned} \quad (30.33)$$

The first term in (30.33) vanishes by integration by parts, $3\langle u_x u^2 \rangle = \langle (u^3)_x \rangle = 0$, and integrating the third term by parts yet again one gets that the energy variation in the Kuramoto-Sivashinsky equation (30.2)

$$\dot{E} = P - D, \quad P = \langle u_x^2 \rangle, \quad D = \langle u_{xxx}^2 \rangle \quad (30.34)$$

balances the power P pumped in by anti-diffusion u_{xx} against the energy dissipation rate D by hyper-viscosity u_{xxxx} .

In figure 30.3 we plot the power input $\langle u_x^2 \rangle$ vs. dissipation $\langle u_{xx}^2 \rangle$ for all $L = 22$ equilibria and relative equilibria determined so far, several periodic orbits and relative periodic orbits, and for a typical ‘turbulent’ evolution. The time averaged energy density \bar{E} computed on a typical orbit goes to a constant, so the mean values (30.27) of drive and dissipation exactly balance each other:

$$\bar{E} = \lim_{t \rightarrow \infty} \frac{1}{t} \int_0^t d\tau \dot{E} = \bar{P} - \bar{D} = 0. \quad (30.35)$$

In particular, the equilibria and relative equilibria fall onto the diagonal in figure 30.3 (a), and so do time averages computed on periodic orbits and relative periodic orbits:

$$E_p = \frac{1}{T_p} \int_0^{T_p} d\tau E(\tau), \quad P_p = \frac{1}{T_p} \int_0^{T_p} d\tau P(\tau) = \bar{D}_p. \quad (30.36)$$

In the Fourier basis (30.32) the conservation of energy on average takes form

$$0 = \sum_{k=-\infty}^{\infty} (q_k^2 - q_k^4) \overline{E}_k, \quad E_k(t) = \frac{1}{2} |a_k(t)|^2. \quad (30.37)$$

The large k convergence of this series is insensitive to the system size L ; \overline{E}_k have to decrease much faster than q_k^{-4} . Deviation of E_k from this bound for small k determines the active modes. This may be useful to bound the number of equilibria, with the upper bound given by zeros of a small number of long wavelength modes.

30.4 Infinite-dimensional flows: Numerics

The computer is not a mere mathematical excrement, useful for technological ends. Rather, I believe that it is a meta-development that might very well change what mathematics is considered to be.

— P. J. Davis [30.13]

The trivial solution $u(x, t) = 0$ is an equilibrium point of (30.2), but that is basically all we know as far as useful analytical solutions are concerned. To develop some intuition about the dynamics we turn to numerical simulations.

How are solutions such as figure 30.1 (b) computed? The salient feature of such partial differential equations is a theorem saying that for state space contracting flows, the asymptotic dynamics is describable by a *finite* set of ‘inertial manifold’ ordinary differential equations. How you solve the equation (30.2) numerically is up to you. Here are some options:

Discrete mesh: You can divide the x interval into a sufficiently fine discrete grid of N points, replace space derivatives in (30.2) by approximate discrete derivatives, and integrate a finite set of first order differential equations for the discretized spatial components $u_j(t) = u(jL/N, t)$, by any integration routine you trust.

Fourier modes: You can integrate numerically the Fourier modes (30.13), truncating the ladder of equations to a finite number of modes N , i.e., set $a_k = 0$ for $k > N$. In the applied mathematics literature more sophisticated variants of such truncations are called *Galerkin truncations*, or *Galerkin projections*. You need to worry about ‘stiffness’ of the equations and the stability of your integrator. For the parameter values explored in this chapter, truncations N in range 16 to 64 yield sufficient accuracy.

exercise 2.6

Pseudo-spectral methods: You can mix the two methods, exploiting the speed of Fast Fourier Transforms.

 example 30.3
p. 585

Figure 30.5: Spatiotemporally periodic solution $u_0(x, t)$, with period $T_0 = 30.0118$. The antisymmetric subspace, $u(x, t) = -u(-x, t)$, so we plot $x \in [0, L/2]$. System size $\tilde{L} = 2.89109$, $N = 16$ Fourier modes truncation. (From ref. [A1.79])

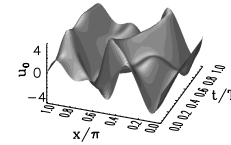
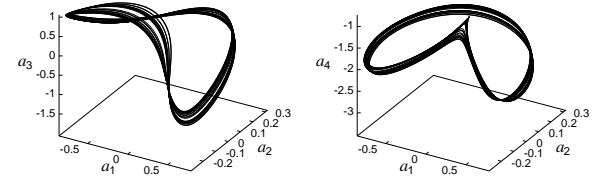


Figure 30.6: Projections of a typical 16-dimensional trajectory onto different 3-dimensional subspaces, coordinates (a) $\{a_1, a_2, a_3\}$, (b) $\{a_1, a_2, a_4\}$. System size $\tilde{L} = 2.89109$, $N = 16$ Fourier modes truncation. (From ref. [A1.79].)



30.5 Visualization

The ultimate goal, however, must be a rational theory of statistical hydrodynamics where [...] properties of turbulent flow can be mathematically deduced from the fundamental equations of hydromechanics.

—E. Hopf

The problem with high-dimensional representations, such as truncations of the infinite tower of equations (30.13), is that the dynamics is difficult to visualize. The best we can do without much programming is to examine the trajectory’s projections onto any three axes a_i, a_j, a_k , as in figure 30.6. example 30.4

The question is: how is one to look at such a flow? It is not clear that restricting the dynamics to a Poincaré section necessarily helps - after all, a section reduces a $(d + 1)$ -dimensional flow to a d -dimensional map, and how much is gained by replacing a continuous flow in 16 dimensions by a set of points in 15 dimensions? The next example illustrates the utility of visualization of dynamics by means of Poincaré sections.

 example 30.4
p. 585

The example 30.4 illustrates why a Poincaré section gives a more informative snapshot of the flow than the full flow portrait. While no fine structure is discernible in the full state space flow portraits of the Kuramoto-Sivashinsky dynamics, figure 30.6, the Poincaré return map figure 30.7 reveals the fractal structure in the asymptotic attractor.

In order to find a better representation of the dynamics, we now turn to its

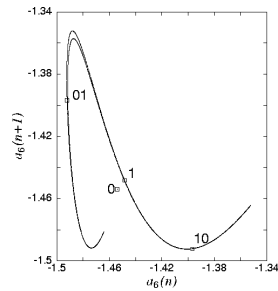


Figure 30.7: The attractor of the Kuramoto-Sivashinsky system (30.13), plotted as the a_6 component of the $a_1 = 0$ Poincaré section return map. Here 10,000 Poincaré section returns of a typical trajectory are plotted. Also indicated are the periodic points 0, 1, 01 and 10. System size $\tilde{L} = 2.89109$, $N = 16$ Fourier modes truncation. (From ref. [A1.79].)

topological invariants.

30.6 Equilibria of equilibria

(Y. Lan and P. Cvitanović)

The set of equilibria and their stable / unstable manifolds form the coarsest topological framework for organizing state space orbits.

The equilibrium condition $u_t = 0$ for the Kuramoto-Sivashinsky equation PDE (30.4) is the ODE

$$\frac{1}{2}(u^2)_x + u_{xx} + u_{xxxx} = 0$$

which can be analyzed as a dynamical system in its own right. Integrating once we get

$$\frac{1}{2}u^2 + u_x + u_{xxx} = c, \tag{30.38}$$

where c is an integration constant whose value strongly influences the nature of the solutions. Written as a 3-dimensional dynamical system with spatial coordinate x playing the role of “time,” this is a volume preserving flow

$$u_x = v, \quad v_x = w, \quad w_x = u^2 - v - c, \tag{30.39}$$

with the “time” reversal symmetry,

$$x \rightarrow -x, \quad u \rightarrow -u, \quad v \rightarrow v, \quad w \rightarrow -w.$$

From (30.39) we see that

$$(u + w)_x = u^2 - c.$$

If $c < 0$, $u + w$ increases without bound with $x \rightarrow \infty$, and every solution escapes to infinity. If $c = 0$, the origin $(0, 0, 0)$ is the only bounded solution.

For $c > 0$ there is much c -dependent interesting dynamics, with complicated fractal sets of bounded solutions. The sets of the solutions of the equilibrium condition (30.39) are themselves in turn organized by the equilibria of the equilibrium condition, and the connections between them. For $c > 0$ the equilibrium points of (30.39) are $c_+ = (\sqrt{c}, 0, 0)$ and $c_- = (-\sqrt{c}, 0, 0)$. Linearization of the flow around c_+ yields Floquet multipliers $[2\lambda, -\lambda \pm i\theta]$ with

$$\lambda = \frac{1}{\sqrt{3}} \sinh \phi, \quad \theta = \cosh \phi,$$

and ϕ fixed by $\sinh 3\phi = 3\sqrt{3}c$. Hence c_+ has a 1-dimensional unstable manifold and a 2-dimensional stable manifold along which solutions spiral in. By the $x \rightarrow -x$ “time reversal” symmetry, the invariant manifolds of c_- have reversed stability properties.

The non-wandering set of this dynamical system is quite pretty, and surprisingly hard to analyze. However, we do not need to explore the fractal set of the Kuramoto-Sivashinsky equilibria for infinite size system here; for a fixed system size L with periodic boundary condition, the only surviving equilibria are those with periodicity L . They satisfy the equilibrium condition for (30.13)

$$q_k^2 (1 - q_k^2) a_k - i \frac{q_k}{2} \sum_{m=-\infty}^{+\infty} a_m a_{k-m} = 0. \tag{30.40}$$

Periods of spatially periodic equilibria are multiples of L . Every time \tilde{L} crosses an integer value $\tilde{L} = n$, new n -cell states are generated through pitchfork bifurcations. In the full state space they form an invariant circle due to the translational invariance of (30.4). In the antisymmetric subspace (see example 30.1), they correspond to two points, half-period translates of each other of the form

$$u(x, t) = -2 \sum_k a_{kn} \sin(knx),$$

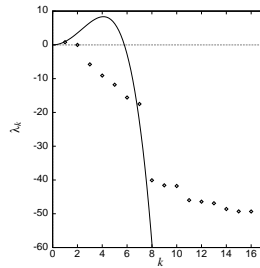
where $a_{kn} \in \mathbb{R}$.

For any fixed spatial period L the number of spatially periodic solutions is finite up to a spatial translation. This observation can be heuristically motivated as follows. Finite dimensionality of the inertial manifold bounds the size of Fourier components of all solutions. On a finite-dimensional compact manifold, an analytic function can only have a finite number of zeros. So, the equilibria, i.e., the zeros of a smooth velocity field on the inertial manifold, are finitely many.

For a sufficiently small L the number of equilibria is small, mostly concentrated on the low wave number end of the Fourier spectrum. These solutions may be obtained by solving the truncated versions of (30.40).

 example 30.7
p. 586

Figure 30.8: Lyapunov exponents $\lambda_{T,k}$ versus k for the least unstable spatio-temporally periodic orbit \bar{T} of the Kuramoto-Sivashinsky system, compared with the Floquet exponents of the $u(x, t) = 0$ stationary solution, $\lambda_k = k^2 - \nu k^4$. The eigenvalue $\lambda_{T,k}$ for $k \geq 8$ falls below the numerical accuracy of integration and are not meaningful. The cycle \bar{T} was computed using methods of chapter 16. System size $\bar{L} = 2.89109$, $N = 16$ Fourier modes truncation. (From ref. [A1.79])



30.7 Why does a flame front flutter?

I understood every word.

—Fritz Haake

section 21.2

We start by considering the case where a_q is an equilibrium point (2.8). Expanding around the equilibrium point a_q , and using the fact that the matrix $A = A(a_q)$ in (4.2) is constant, we can apply the simple formula (5.1) also to the Jacobian matrix of an equilibrium point of a PDE,

$$J^t(a_q) = e^{At} \quad A = A(a_q).$$

For $\bar{L} < 1$, $u(x, t) = 0$ is the globally attractive stable equilibrium. As the system size \bar{L} is increased, the “flame front” becomes increasingly unstable and turbulent, the dynamics goes through a rich sequence of bifurcations on which we shall not dwell here.

The long wavelength perturbations of the flat-front equilibrium are linearly unstable, while all short wavelength perturbations are strongly contractive. The high k eigenvalues, corresponding to rapid variations of the flame front, decay so fast that the corresponding eigen-directions are physically irrelevant. To illustrate the rapid contraction in the non-leading eigen-directions we plot in figure 30.8 the eigenvalues of the equilibrium in the unstable regime, for relatively small system size, and compare them with the Floquet multipliers of the least unstable cycle for the same system size. The equilibrium solution is very unstable, in 5 eigen-directions, the least unstable cycle only in one. Note that for $k > 7$ the rate of contraction is so strong that higher eigen-directions are numerically meaningless for either solution; even though the flow is infinite-dimensional, the attracting set must be rather thin.

While in general for \bar{L} sufficiently large one expects many coexisting attractors in the state space, in numerical studies most random initial conditions seem to settle on the same chaotic attractor.

From (30.13) we see that the equilibrium $u(x, t) = 0$ has Fourier modes as the linear stability eigenvectors. For $|k| < \bar{L}$, the corresponding Fourier modes

are unstable. The most unstable mode has $k = \bar{L}/\sqrt{2}$ and defines the scale of basic building blocks of the spatiotemporal dynamics of the Kuramoto-Sivashinsky equation in large system size limit.

Consider now the case of initial a_k sufficiently small that the bilinear $a_m a_{k-m}$ terms in (30.13) can be neglected. Then we have a set of decoupled linear equations for a_k whose solutions are exponentials, at most a finite number for which $k^2 > \nu k^4$ is growing with time, and infinitely many with $\nu k^4 > k^2$ decaying in time. The growth of the unstable long wavelengths (low $|k|$) excites the short wavelengths through the $a_m a_{k-m}$ nonlinear term. The excitations thus transferred are dissipated by the strongly damped short wavelengths, and a “chaotic equilibrium” can emerge. The very short wavelengths $|k| \gg 1/\sqrt{\nu}$ remain small for all times, but the intermediate wavelengths of order $|k| \sim 1/\sqrt{\nu}$ play an important role in maintaining the dynamical equilibrium. As the damping parameter decreases, the solutions increasingly take on shock front character poorly represented by the Fourier basis, and many higher harmonics may need to be kept in truncations of (30.13).

Hence, while one may truncate the high modes in the expansion (30.13), care has to be exercised to ensure that no modes essential to the dynamics are chopped away.

In other words, even though our starting point (30.2) is an infinite-dimensional dynamical system, the asymptotic dynamics unfolds on a finite-dimensional attracting manifold, and so we are back on the familiar territory of sect. 2.2: the theory of a finite number of ODEs applies to this infinite-dimensional PDE as well.

We can now start to understand the remark on page 43 that for infinite dimensional systems time reversibility is not an option: evolution forward in time strongly damps the higher Fourier modes. There is no turning back: if we reverse the time, the infinity of high modes that contract strongly forward in time now explodes, instantly rendering evolution backward in time meaningless. As so much you are told about dynamics, this claim is also wrong, in a subtle way: if the initial $u(x, 0)$ is in the non-wandering set (2.3), the trajectory is well defined both forward and backward in time. For practical purposes, this subtlety is not of much use, as any time-reversed numerical trajectory in a finite-mode truncation will explode very quickly, unless special precautions are taken.

When is an equilibrium important? There are two kinds of roles equilibria play:

“Hole” in the natural measure. The more unstable eigen-directions it has (for example, the $u = 0$ solution), the more unlikely it is that an orbit will recur in its neighborhood.

Unstable manifold of a “least unstable” equilibrium. Asymptotic dynamics spends a large fraction of time in neighborhoods of a few equilibria with only a few unstable eigen-directions.

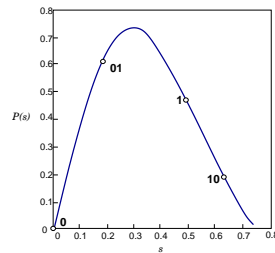


Figure 30.9: The Poincaré return map of the Kuramoto-Sivashinsky system (30.13) figure 30.7, from the unstable manifold of the $\bar{1}$ fixed point to the (neighborhood of) the unstable manifold. Also indicated are the periodic points $\bar{0}$ and $\bar{01}$.

30.8 Intrinsic parametrization

Both in the Rössler flow of example 3.3, and in the Kuramoto-Sivashinsky system of example 30.4 we have learned that the attractor is very thin, but otherwise the return maps that we found were disquieting – neither figure 3.3 nor figure 30.7 appeared to be one-to-one maps. This apparent loss of invertibility is an artifact of projection of higher-dimensional return maps onto lower-dimensional subspaces. As the choice of lower-dimensional subspace is arbitrary, the resulting snapshots of return maps look rather arbitrary, too. Other projections might look even less suggestive.

Such observations beg a question: Does there exist a ‘natural’, intrinsically optimal coordinate system in which we should plot of a return map?

As we shall now argue (see also sect. 16.1), the answer is yes: The intrinsic coordinates are given by the stable/unstable manifolds, and a return map should be plotted as a map from the unstable manifold back onto the immediate neighborhood of the unstable manifold.

Examination of numerical plots such as figure 30.6 suggests that a more thoughtful approach would be to find a coordinate transformation $y = h(x)$ to a ‘center manifold’, such that in the new, curvilinear coordinates large-scale dynamics takes place in (y_1, y_2) coordinates, with exponentially small dynamics in y_3, y_4, \dots . But - thinking is extra price - we do not know how to actually accomplish this, and we do not believe it can be accomplished globally.

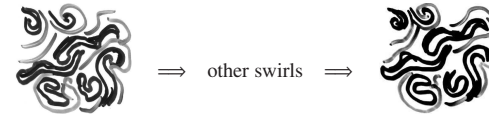
Both in the example of the Rössler flow and of the Kuramoto-Sivashinsky system we sketched the attractors by running a long chaotic trajectory, and noted that the attractors are very thin, but otherwise the return maps that we plotted were disquieting – neither figure 3.3 nor figure 30.7 appeared to be 1-to-1 maps. In this section we show how to use such information to approximately locate cycles.

Résumé

Turbulence is the graveyard of theories
— Hans W. Liepmann

We have learned that an instanton is an analytic solution of Yang-Mills equations of motion, but shouldn’t a strongly nonlinear field theory dynamics be dominated by turbulent solutions? How are we to think about systems where every spatiotemporal solution is unstable?

Here we think of turbulence in terms of *recurrent* spatiotemporal patterns. Pictorially, dynamics drives a given spatially extended system through a repertoire of unstable patterns; as we watch a turbulent system evolve, every so often we catch a glimpse of a familiar pattern:



For a finite spatial resolution and a finite time, a pattern belonging to a finite alphabet of admissible patterns is observed; the long term dynamics can be thought of as a walk through the space of such patterns. Recasting this image into mathematics is what ChaosBook is about.

The problem one faces with high-dimensional flows is that their topology is hard to visualize, and that even with a decent starting guess for a point on a periodic orbit, methods like the Newton-Raphson method are likely to fail. Methods that start with initial guesses for a number of points along the cycle, such as the multipoint shooting method of sect. 16.2, are more robust. The relaxation (or variational) methods take this strategy to its logical extreme, and start by a guess of not a few points along a periodic orbit, but a guess of the entire orbit. As these methods are intimately related to variational principles and path integrals, we postpone their introduction to chapter 33.

chapter 33

At present the theory is in practice applicable only to systems with a low *intrinsic dimension* – the minimum number of coordinates necessary to capture its essential dynamics. If the system is very turbulent (a description of its long time dynamics requires a space of very high intrinsic dimension) we are out of luck.

Commentary

Remark 30.1 A brief history of dynamicist’s vision of turbulence. Dynamical approaches to study of turbulence are - surprisingly - still a cutting-edge research area. You might find Appendix A1.5 amusing. The Kuramoto-Sivashinsky equation was introduced in refs. [A1.75, A1.76]. Holmes, Lumley and Berkooz [A1.74] offer a delightful discussion of why this system deserves study as a staging ground for studying turbulence in full-fledged Navier-Stokes equation. How good a description of a flame front this equation is not a concern here; suffice it to say that such model amplitude equations for interfacial instabilities arise in a variety of contexts - see e.g. ref. [30.17] - and this one is perhaps the simplest physically interesting spatially extended nonlinear system.

The work described in this chapter was initiated by Putkaradze's 1996 ChaosBook term project (see ChaosBook.org/extras), and continued by Budanur, Christiansen, Cvitanović, Davidchack, Ding, Lan, and Siminos [A1.79, 32.70, A1.83, 33.16, 33.15, A1.84, 30.5, 30.23].

30.9 Examples

Example 30.1 Kuramoto-Sivashinsky antisymmetric subspace: The Fourier coefficients a_k are in general complex numbers. We can isolate the antisymmetric subspace $u(x, t) = -u(-x, t)$ by considering the case of a_k pure imaginary, $a_k \rightarrow ia_k$, where $a_k = -a_{-k}$ are real, with the evolution equations

$$\dot{a}_k = q_k^2 (1 - q_k^2) a_k + \frac{q_k}{2} \sum_{m=-\infty}^{+\infty} a_m a_{k-m}. \tag{30.41}$$

By picking this subspace we eliminate the continuous translational symmetry from our considerations; that is not an option for an experimentalist, but will do for our purposes. In the antisymmetric subspace the translational invariance of the full system reduces to the invariance under discrete translation by half a spatial period L . In the Fourier representation (30.41) this corresponds to invariance under

$$a_{2m} \rightarrow a_{2m}, a_{2m+1} \rightarrow -a_{2m+1}. \tag{30.42}$$

click to return: p. ??

Example 30.2 Cyclic subgroups of $SO(2)$: Any rational shift $\tau_{1/m} u(x) = u(x + L/m)$ generates a discrete cyclic subgroup C_m of $O(2)$, also a symmetry of KS system. Reflection together with C_m generates another symmetry of KS system, the dihedral subgroup D_m of $O(2)$. The only non-zero Fourier components of a solution invariant under C_m are $a_{jm} \neq 0$, $j = 1, 2, \dots$, while for a solution invariant under D_m we also have the condition $\text{Re } a_j = 0$ for all j . D_m reduces the dimensionality of state space and aids computation of equilibria and periodic orbits within it. For example, the 1/2-cell translations

$$\tau_{1/2} u(x) = u(x + L/2) \tag{30.43}$$

and reflections generate $O(2)$ subgroup $D_2 = \{1, \sigma, \tau, \tau\sigma\}$, which reduces the state space into four irreducible subspaces (for brevity, here $\tau = \tau_{1/2}$):

$$\begin{matrix} & & \tau & \sigma & \tau\sigma \\ P^{(1)} & = & \frac{1}{4}(1 + \tau + \sigma + \tau\sigma) & S & S & S \\ P^{(2)} & = & \frac{1}{4}(1 + \tau - \sigma - \tau\sigma) & S & A & A \\ P^{(3)} & = & \frac{1}{4}(1 - \tau + \sigma - \tau\sigma) & A & S & A \\ P^{(4)} & = & \frac{1}{4}(1 - \tau - \sigma + \tau\sigma) & A & A & S. \end{matrix} \tag{30.44}$$

$P^{(j)}$ is the projection operator onto $u^{(j)}$ irreducible subspace, and the last 3 columns refer to the symmetry (or antisymmetry) of $u^{(j)}$ functions under reflection and 1/2-cell

shift. By the same argument that identified (30.11) as the invariant subspace of KS, here the KS flow stays within the $\mathbb{U}^S = \mathbb{U}^{(1)} + \mathbb{U}^{(2)}$ irreducible D_1 subspace of u profiles symmetric under 1/2-cell shifts.

While in general the bilinear term $(u^2)_x$ mixes the irreducible subspaces of D_n , for D_2 there are four subspaces invariant under the flow [30.17]:

- {0}: the $u(x) = 0$ equilibrium
- $\mathbb{U}^+ = \mathbb{U}^{(1)} + \mathbb{U}^{(3)}$: the reflection D_1 irreducible space of antisymmetric $u(x)$
- $\mathbb{U}^S = \mathbb{U}^{(1)} + \mathbb{U}^{(2)}$: the shift D_1 irreducible space of $L/2$ shift symmetric $u(x)$
- $\mathbb{U}^{(1)}$: the D_2 irreducible space of $u(x)$ invariant under $x \mapsto L/2 - x$, $u \mapsto -u$.

With the continuous translational symmetry eliminated within each subspace, there are no relative equilibria and relative periodic orbits, and one can focus on the equilibria and periodic orbits only, as was done for \mathbb{U}^+ in refs. [A1.79, A1.83, 30.23]. In the Fourier representation, the $u \in \mathbb{U}^+$ antisymmetry amounts to having purely imaginary coefficients, since $a_{-k} = a_k^* = -a_k$. The 1/2 cell-size shift $\tau_{1/2}$ generated 2-element discrete subgroup $\{1, \tau_{1/2}\}$ is of particular interest because in the \mathbb{U}^+ subspace the translational invariance of the full system reduces to invariance under discrete translation (30.43) by half a spatial period $L/2$.

Each of the above dynamically invariant subspaces is unstable under small perturbations, and generic solutions of Kuramoto-Sivashinsky equation belong to the full space. Nevertheless, since all equilibria of the KS flow studied in this paper lie in the \mathbb{U}^+ subspace (see sect. ??), \mathbb{U}^+ plays important role for the global geometry of the flow. However, linear stability of these equilibria has eigenvectors both in and outside of \mathbb{U}^+ , and needs to be computed in the full state space.

click to return: p. ??

Example 30.3 Kuramoto-Sivashinsky simulation, antisymmetric subspace: To get started, we set $\nu = 0.029910$, $L = 2\pi$ in the Kuramoto-Sivashinsky equation (30.2), or, equivalently, $\nu = 1$, $L = 36.33052$ in the non-dimensionalized (30.41). Consider the antisymmetric subspace (30.41), so the non-dimensionalized system size is $\tilde{L} = L/2\pi = 2.89109$. Truncate (30.41) to $0 \leq k \leq 16$, and integrate an arbitrary initial condition. Let the transient behavior settle down.

Why this \tilde{L} ? For this system size \tilde{L} the dynamics appears to be chaotic, as far as can be determined numerically. Why $N = 16$? In practice one repeats the same calculation at different truncation cutoffs N , and makes sure that the inclusion of additional modes has no effect within the desired accuracy. For this system size $N = 16$ suffices.

Once a trajectory is computed in Fourier space, we can recover and plot the corresponding spatiotemporal pattern $u(x, t)$ over the configuration space using (2.16), as in figure 30.1 (b) and figure 30.5. Such patterns give us a qualitative picture of the flow, but no detailed dynamical information; for that, tracking the evolution in a high-dimensional state space, such as the space of Fourier modes, is much more informative.

click to return: p. ??

Example 30.4 Kuramoto-Sivashinsky Poincaré return maps: Consider the Kuramoto-Sivashinsky equation in the N Fourier modes representation. We pick (arbitrarily) the hyperplane $a_1 = 0$ as the Poincaré section, and integrate (30.13) with $a_1 = 0$, and an arbitrary initial point (a_2, \dots, a_N) . When the flow crosses the $a_1 = 0$ hyperplane in the same direction as initially, the initial point is mapped into $(a_2', \dots, a_N') = P(a_2, \dots, a_N)$.

Table 30.1: Important Kuramoto-Sivashinsky equilibria: the first few Floquet exponents

S	$\mu^{(1)} \pm i\omega^{(1)}$	$\mu^{(2)} \pm i\omega^{(2)}$	$\mu^{(3)} \pm i\omega^{(3)}$
C_1	$0.04422 \pm i0.26160$	$-0.255 \pm i0.431$	$-0.347 \pm i0.463$
R_1	$0.01135 \pm i0.79651$	$-0.215 \pm i0.549$	$-0.358 \pm i0.262$
T	0.25480	$-0.07 \pm i0.645$	-0.264

This defines P , the Poincaré return map (3.1) of the $(N - 1)$ -dimensional $a_1 = 0$ hyperplane into itself.

Figure 30.7 is a typical result. We have picked - again arbitrarily - a subspace such as $a_6(n + 1)$ vs. $a_6(n)$ in order to visualize the dynamics. While the topology of the attractor is still obscure, one thing is clear: even though the flow state space is infinite dimensional, the attractor is finite and thin, barely thicker than a line. click to return: p. ??

Example 30.5 Stability matrix, antisymmetric subspace: The Kuramoto-Sivashinsky flat flame front $u(x, t) = 0$ is an equilibrium point of (30.2). The stability matrix (4.3) follows from (30.13)

$$A_{kj}(a) = \frac{\partial v_k(a)}{\partial a_j} = (q_k^2 - q_k^4)\delta_{kj} + q_k(a_{k-j} - a_{k+j}). \quad (30.45)$$

For the $u(x, t) = 0$ equilibrium solution the stability matrix is diagonal, the eigenvalues are Fourier modes, and - as in (4.32) - the Jacobian matrix is diagonal, $J'_{kj}(0) = \delta_{kj}e^{(q_k^2 - q_k^4)t}$.

Example 30.6 Stability of Kuramoto-Sivashinsky equilibria:

spiraling out in a plane, all other directions contracting

Stability of ‘center’ equilibrium

linearized Floquet exponents:

$$(\mu^{(1)} \pm i\omega^{(1)}, \mu^{(2)} \pm i\omega^{(2)}, \dots) = (0.044 \pm i0.262, -0.255 \pm i0.431, \dots)$$

The plane spanned by $\mu^{(1)} \pm i\omega^{(1)}$ eigenvectors rotates with angular period $T \approx 2\pi/\omega^{(1)} = 24.02$.

a trajectory that starts near the C_1 equilibrium point spirals away per one rotation with multiplier $\Lambda_{radial} \approx \exp(\mu^{(1)}T) = 2.9$.

each Poincaré section return, contracted into the stable manifold by factor of $\Lambda_2 \approx \exp(\mu^{(2)}T) = 0.002$

The local Poincaré return map is in practice 1 - dimensional

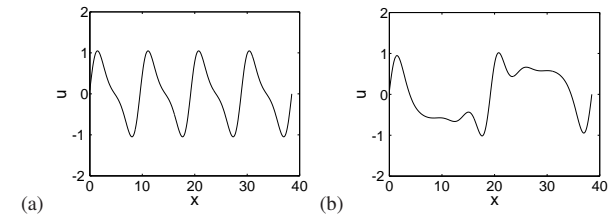
click to return: p. ??

Example 30.7 Some Kuramoto-Sivashinsky equilibria:

See figure 30.10.

click to return: p. ??

Figure 30.10: The non-wandering set under study appears to consist of three patches: the left part (S_L), the center part (S_C) and the right part (S_R), each centered around an unstable equilibrium: (a) central C_1 equilibrium, (b) side R_1 equilibrium on the interval $[0, L]$.



Exercises

30.1. Galilean invariance of the Kuramoto-Sivashinsky equation.

- (a) Verify that the Kuramoto-Sivashinsky equation is Galilean invariant: if $u(x, t)$ is a solution, then $v + u(x + 2vt, t)$, with v an arbitrary constant velocity, is also a solution.

- (b) Verify that mean

$$\langle u \rangle = \frac{1}{L} \int_L dx u$$

is conserved by the flow.

- (c) Argue that the choice (30.3) of the vanishing mean velocity, $\langle u \rangle = 0$ leads to no loss of generality in calculations that follow.

- (d) [thinking is extra cost] Inspection of various “turbulent” solutions of Kuramoto-Sivashinsky equation reveals subregions of “traveling waves” with locally nonzero $\langle u \rangle$. Is there a way to use Galilean invariance locally, even though we eliminated it by the $\langle u \rangle = 0$ condition?

30.2. Infinite dimensional dynamical systems are not smooth. Many of the operations we consider natural for finite dimensional systems do not have smooth behavior in infinite dimensional vector spaces. Consider, as an example, a concentration ϕ diffusing on \mathbb{R} according to the diffusion equation

$$\partial_t \phi = \frac{1}{2} \nabla^2 \phi.$$

- (a) Interpret the partial differential equation as an infinite dimensional dynamical system. That is, write it as $\dot{x} = F(x)$ and find the velocity field.

- (b) Show by examining the norm

$$\|\phi\|^2 = \int_{\mathbb{R}} dx \phi^2(x)$$

that the vector field F is not continuous.

- (c) Try the norm

$$\|\phi\| = \sup_{x \in \mathbb{R}} |\phi(x)|.$$

Is F continuous?

- (d) Argue that the semi-flow nature of the problem is not the cause of our difficulties.
- (e) Do you see a way of generalizing these results?

30.3. Kuramoto-Sivashinsky energy transfer rates.

- (a) Derive (30.31) from (30.30). Now that you have your integration by parts skills hone, also show that

$$\begin{aligned} \langle u_{xxx}u^2 \rangle &= \langle u_x^3 \rangle \\ \langle u_{xxxx}u^2 \rangle &= -5\langle u_x u_{xx}^2 \rangle. \end{aligned} \quad (30.46)$$

- (b) Derive the power - dissipation rate relation (30.34).

- (c) Prove that for an equilibrium E is constant.

- (d) Derive formulas for \dot{P} , \dot{D} , \dot{E} and $\frac{d}{dt} \langle u_x^3 \rangle$ in terms of space averages $\langle \dots \rangle$. You will note that higher derivatives of u appear. The guiding principle is to use integration by parts until the number of such derivatives is minimized.

- (e) Invent another such formula.

30.4. Navier-Stokes energy transfer rates. The Millennium Prize tempts you to ponder the Navier-Stokes equations

$$\partial_t v_i + v_j \partial_j v_i = -\partial_i p + \nu \partial_{jj} v_i \quad (30.47)$$

in the utterly unphysical setting, a periodic 3D box of size $[L \times L \times L]$. The space average of a function $a = a(x, t) = a(v(x, t))$ on the interval L is given by

$$\langle a \rangle = \frac{1}{L^3} \oint dx^3 a(x, t). \quad (30.48)$$

- (a) Prove conservation of momentum

$$\frac{d}{dt}\langle v_i \rangle = 0 \quad (30.49)$$

- (b) Prove power-dissipation rate relation

$$\frac{1}{2} \frac{d}{dt} \langle v^2 \rangle = -\nu \langle |\omega|^2 \rangle \quad (30.50)$$

- (c) Prove conservation of helicity.

$$\frac{1}{2} \frac{d}{dt} \langle v \cdot \omega \rangle = -\nu \langle \omega \cdot \nabla \times \omega \rangle \quad (30.51)$$

- (d) While you are on the roll: derive another such formula. Pipe or plane Couette flow power-dissipation relation
- $\dot{E} = P - D$
- would be particularly useful.

30.5. Local Galilean invariance of Kuramoto-Sivashinsky?



Inspection of various “turbulent” solutions of Kuramoto-Sivashinsky equation reveals subregions of “traveling waves” with locally nonzero $\langle u \rangle$. Is there a way to use Galilean invariance locally, even though we eliminated it by the $\langle u \rangle = 0$ condition?

References

- [30.1] P. Cvitanović, R. L. Davidchack, and E. Siminos, On the state space geometry of the Kuramoto-Sivashinsky flow in a periodic domain, *SIAM J. Appl. Dyn. Syst.* **9**, 1 (2010), arXiv:0709.2944.
- [30.2] Y. Kuramoto and T. Tsuzuki, Persistent propagation of concentration waves in dissipative media far from thermal equilibrium, *Progr. Theor. Phys.* **55**, 365 (1976).
- [30.3] G. I. Sivashinsky, Nonlinear analysis of hydrodynamical instability in laminar flames - I. Derivation of basic equations, *Acta Astronaut.* **4**, 1177 (1977).
- [30.4] I. G. Kevrekidis, B. Nicolaenko, and J. C. Scovel, Back in the saddle again: a computer assisted study of the Kuramoto-Sivashinsky equation, *SIAM J. Appl. Math.* **50**, 760 (1990).
- [30.5] J. F. Gibson, J. Halcrow, and P. Cvitanović, Visualizing the geometry of state-space in plane Couette flow, *J. Fluid Mech.* **611**, 107 (2008), arXiv:0705.3957.
- [30.6] J. F. Gibson, *Movies of plane Couette* (Georgia Tech, 2009); Chaos-Book.org/tutorials.
- [30.7] O. Reynolds. An experimental investigation of the circumstances which determine whether the motion of water shall be direct or sinuous, and the law of resistance in parallel channels. *Proc. Roy. Soc. Lond. Ser A*, 174:935–982, 1883.
- [30.8] W. M. F. Orr. The stability or instability of the steady motions of a liquid. Part II: A viscous liquid. *Proc. Roy. Irish Acad. A*, 27:69–138, 1907.
- [30.9] J. M. Greene and J.-S. Kim, The steady states of the Kuramoto-Sivashinsky equation, *Physica D* **33**, 99 (1988).
- [30.10] G. Kawahara and S. Kida. Periodic motion embedded in plane Couette turbulence: Regeneration cycle and burst. *J. Fluid Mech.*, 449:291–300, 2001.
- [30.11] T. J. Bridges, private communication.
- [30.12] U. Frisch, *Turbulence* (Cambridge Univ. Press, Cambridge, 1996).
- [30.13] P. J. Davis, “Spanning multiple worlds,” *SIAM News* **41** (Dec. 2008).
- [30.14] C. Foias, B. Nicolaenko, G.R. Sell, and R. Témam, “Kuramoto-Sivashinsky equation,” *J. Math. Pures et Appl.* **67**, 197 (1988).
- [30.15] F. Christiansen, P. Cvitanović and V. Putkaradze, “Spatiotemporal chaos in terms of unstable recurrent patterns,” *Nonlinearity* **10**, 55 (1997); arXiv:chao-dyn/9606016.
- [30.16] P. Holmes, J.L. Lumley and G. Berkooz, *Turbulence, Coherent Structures, Dynamical Systems and Symmetry* (Cambridge U. Press, Cambridge 1996).
- [30.17] I.G. Kevrekidis, B. Nicolaenko and J.C. Scovel, “Back in the saddle again: a computer assisted study of the Kuramoto-Sivashinsky equation,” *SIAM J. Applied Math.* **50**, 760 (1990).
- [30.18] D. Michelson, Steady solutions of the Kuramoto-Sivashinsky equation, *Physica D* **19**, 89 (1986).
- [30.19] L. Giacomelli and F. Otto, New bounds for the Kuramoto-Sivashinsky equation, *Comm. Pure Appl. Math.* **58**, 297 (2005).
- [30.20] J. C. Bronski and T. N. Gambill, Uncertainty estimates and L_2 bounds for the Kuramoto-Sivashinsky equation, *Nonlinearity* **19**, 2023–2039 (2006); arXiv:math/0508481.
- [30.21] “Chaotic field theory: a sketch,” *Physica A* **288**, 61 (2000); arXiv:nlin.CD/0001034.
- [30.22] Y. Lan, *Dynamical systems approach to 1-d spatiotemporal chaos – A cyclist’s view*, Ph.D. thesis, Georgia Inst. of Tech. (2004).
- [30.23] Y. Lan and P. Cvitanović, “Unstable recurrent patterns in Kuramoto-Sivashinsky dynamics,” *Phys. Rev. E* **78**, 026208 (2004); arXiv:0804.2474.
- [30.24] A. K. Kassam and L. N. Trefethen, “Fourth-order time stepping for stiff PDEs,” *SIAM J. Sci. Comp.*, (2004).
- [30.25] Poul Martin Møller, *En dansk Students Eventyr [The Adventures of a Danish Student]* (Copenhagen 1824).
- [30.26] H. K. Moffatt, Fixed points of turbulent dynamical systems and suppression of nonlinearity, Comment 1, in *Whither Turbulence! Turbulence at the Crossroads*, edited by J. L. Lumley, pp. 250–257, Springer, New York, 1990.

- [30.27] J. M. Hamilton, J. Kim, and F. Waleffe, Regeneration mechanisms of near-wall turbulence structures, *J. Fluid Mech.* **287**, 317 (1995).
- [30.28] F. Waleffe, Hydrodynamic stability and turbulence: Beyond transients to a Self-Sustaining Process, *Stud. Applied Math.* **95**, 319 (1995).
- [30.29] F. Waleffe, On a Self-Sustaining Process in shear flows, *Phys. Fluids* **9**, 883 (1997).
- [30.30] F. Waleffe, Three-dimensional coherent states in plane shear flows, *Phys. Rev. Lett.* **81**, 4140 (1998).
- [30.31] F. Waleffe, Exact coherent structures in channel flow, *J. Fluid Mech.* **435**, 93 (2001).
- [30.32] F. Waleffe, Homotopy of exact coherent structures in plane shear flows, *Phys. Fluids* **15**, 1517 (2003).
- [30.33] R. M. Clever and F. H. Busse, Three-dimensional convection in a horizontal layer subjected to constant shear, *J. Fluid Mech.* **234**, 511 (1992).
- [30.34] H. Faisst and B. Eckhardt, Traveling waves in pipe flow, *Phys. Rev. Lett.* **91**, 224502 (2003).
- [30.35] H. Wedin and R. R. Kerswell, Exact coherent structures in pipe flow: Traveling wave solutions, *J. Fluid Mech.* **508**, 333 (2004).